

Dipolar phonons and electronic screening in monolayer FeSe on SrTiO₃

Yuanjun Zhou and Andrew J. Millis

Department of Physics, Columbia University, New York, New York 10027, USA

(Dated: February 6, 2020)

Monolayer films of FeSe grown on SrTiO₃ substrates exhibit significantly higher superconducting transition temperatures than those of bulk FeSe. Interaction of electrons in the FeSe layer with dipolar SrTiO₃ phonons has been suggested as the cause of the enhanced transition temperature. In this paper we systematically study the coupling of SrTiO₃ longitudinal optical phonons to the FeSe electron, including also electron-electron Coulomb interactions at the random phase approximation level. We find that the electron-phonon interaction between FeSe and SrTiO₃ substrate is almost entirely screened by the electronic fluctuations in the FeSe monolayer, so that the net electron-phonon interaction is very weak and unlikely to lead to superconductivity.

I. INTRODUCTION

The recent discovery of superconductivity, or its signatures at temperatures of orders 70K (tunneling measurements) and 100K (*in situ* four-point measurements) in monolayers of FeSe grown on the (001) and (111) surfaces of niobium-doped SrTiO₃(STO)¹⁻³ challenges our understanding of superconductivity in the pnictide compounds and has stimulated intense research activity. Monolayer FeSe on STO is heavily electron doped relative to bulk FeSe⁴. Surface potassium doping of free-standing FeSe films^{5,6} produces transition temperatures as high as 45K, and systematic variation of carrier concentration using gate doping with liquid dielectrics reveals that the high transition temperature appears at the point where the doping is large enough to eliminate the zone center hole pockets⁷. However, the highest transition temperatures induced by pure electron doping are about 45K, still notably less than the 70K or 100K³ reported for monolayer FeSe on STO, and recent studies of monolayer FeSe on anatase TiO₂ report similarly high transition temperatures⁸, strongly suggesting that an additional substrate-specific T_c enhancement occurs. One clue to the nature of the substrate-specific interactions is provided by recent angle-resolved photoemission spectroscopy (ARPES) measurements⁹, which reveal “replica” bands, images of the FeSe conduction band shifted up in binding energy by an amount comparable to one of the longitudinal optical (LO) phonon energies in SrTiO₃. These bands are attributed to interaction of electrons in the FeSe with very long wavelength optical phonons in the SrTiO₃.

Theoretical papers have appeared analyzing the interfacial enhancement of the T_c and the presence of replica bands in monolayer FeSe on STO via the electron - LO phonon interaction^{10,11}. However, these studies focus mainly on the electron phonon interaction, neglecting the Coulomb interaction between the FeSe electrons. This interaction may screen the electron-phonon interaction. In an extreme antiadiabatic limit and with Thomas-Fermi screening, Gor'kov¹² recently studied the electron phonon interactions in the FeSe/STO system and argued that the LO phonons from STO are not enough to induce

such a high T_c found in the FeSe/STO system.

In this paper, we present an analysis that treats the STO LO phonons and the FeSe Coulomb interaction on an equal footing. We find that although the LO phonons in STO generates an attractive potential, it is strongly screened by the electrons in FeSe layer, so that the electron-phonon interaction suppressed, producing neither replica bands nor an appreciable contribution to superconductivity for reasonable parameters. This is similar to the result found in Inkson and Anderson on plasmon-mediated superconductivity.¹³

The paper is organized as follows. Section II presents the screened electron phonon interaction in FeSe/STO. Section III gives a RPA level analysis of the total interaction. Section IV discusses the 2D plasmons in FeSe. Section V analyses the net phonon contribution to the electron-electron interaction. In section VI we discuss the possibility of replica bands. Finally Section VII is a summary and conclusion. Appendices give details of derivations.

II. ELECTRON-PHONON INTERACTION

We consider a monolayer of FeSe grown on top of a semi-infinite SrTiO₃ crystal. We take the STO to occupy the $z < 0$ half-plane and assume that the electrons in the FeSe occupy a layer of negligible thickness at a distance $z_1 > 0$ from the surface. In the actual system, $z_1 \approx 4.3\text{\AA}$. In the SrTiO₃ we consider that each unit cell i hosts several atomic displacement modes, labelled by an index a and characterized by a displacement vector \vec{d}_i^a with effective charge $Z_a e$ (e is the electron charge) so the dipole moment due to a given ionic displacement is $Z_a \vec{d}_i^a$. We Fourier transform on the in-plane coordinates and label the planes parallel to the interface by J so that the dipole moment is $Z_a \vec{d}(q)_J^a$. In FeSe we focus on the electronic charge density $-e\rho$ which we write as a function of the in-plane momentum q .

To derive the Hamiltonian we write the total Coulomb energy as

$$H_{Coul} = \int \frac{d^2q}{(2\pi)^2} \mathcal{H}_{DD}(q) + \mathcal{H}_{D\rho}(q) + \mathcal{H}_{\rho\rho}(q) \quad (1)$$

with

$$\mathcal{H}_{DD}(q) = \frac{1}{2} \sum_{JJ'ab} V_{DD}(J, J', q) Z_a Z_b d(q)_J^a d(-q)_{J'}^b \quad (2)$$

$$\mathcal{H}_{D\rho}(q) = \sum_{Ja} V_{D\rho}(J, q) Z_a d(q)_J^a \rho(-q) \quad (3)$$

$$\mathcal{H}_{\rho\rho}(q) = \frac{1}{2} V_{\rho\rho}(q) \rho(q) \rho(-q) \quad (4)$$

where $V_{DD}(q, (J, J', q))$ gives the interaction energy between dipoles of unit charge and in-plane momentum q in layers J, J' , etc.

Determining the interactions V requires solving an electrostatics problem that is complicated by the spatial asymmetry (vacuum at $z > z_1$ and SrTiO₃ at $z < 0$) and the lack of momentum conservation in the z direction. However, useful simplifications occur in the long wavelength limit of interest here. Details are given in Appendix A. The results depend on three effective dielectric constants: ϵ_1 parametrizing the strength of an electric field in the FeSe layer due to charges in this layer, ϵ_2 parametrizing the strength of an electric field in the STO due to charges in the STO and ϵ_* describing the field in the FeSe layer due to a charge in the STO. The dependence of the effective dielectric constant on wavevector is shown in Fig. 1 (this dependence is not denoted explicitly in the formulas that follow.) Important parameters of ϵ_1, ϵ_2 and ϵ_* are ϵ_{STO} , and ϵ_{FeSe} . ϵ_{STO} is the ‘‘high frequency’’ dielectric constant of the STO, formally defined as the bulk STO dielectric constant at frequencies much less than the SrTiO₃ band gap, if the dipolar phonons are frozen. Similarly, ϵ_{FeSe} is the dielectric constant of FeSe if the electronic charge fluctuations are frozen. Detailed formulas are in the Appendix A and the asymptotics are in Table I (note in particular the simplicity of the long wavelength limit, in which half of the field lines are in vacuum and half in the STO). Note that the high frequency dielectric constants ϵ_{FeSe} and ϵ_{STO} are both small^{14–16} and the intrinsic momentum dependences of ϵ_1, ϵ_2 and ϵ_* are weak.

TABLE I. Asymptotics of dielectric constants.

	$qz_1 \sim 0$	$qz_1 \sim \infty$
ϵ_1	$(\epsilon_{\text{STO}} + 1)/2$	$(\epsilon_{\text{FeSe}} + 1)/2$
ϵ_2	$(\epsilon_{\text{STO}} + 1)/2$	$(\epsilon_{\text{STO}} + \epsilon_{\text{FeSe}})/2$
ϵ_*	$(\epsilon_{\text{STO}} + 1)/2$	$(\epsilon_{\text{STO}} + \epsilon_{\text{FeSe}})(\epsilon_{\text{FeSe}} + 1)/4\epsilon_{\text{FeSe}}$

After solving the electrostatic problem and integrating out the phonons (see Appendix B) we obtain a Lagrangian describing the electron density fluctuations screened by the STO longitudinal phonons as

$$\mathcal{L}_{el} = \frac{1}{2} \int \frac{d^2q}{(2\pi)^2} \rho_q \rho_{-q} V_{\text{eff}}(q, \Omega) \quad (5)$$

with effective electron-electron interaction

$$V_{\text{eff}}(q, \Omega) = \frac{2\pi e^2}{q\epsilon_{ion}(q, \Omega)} \quad (6)$$

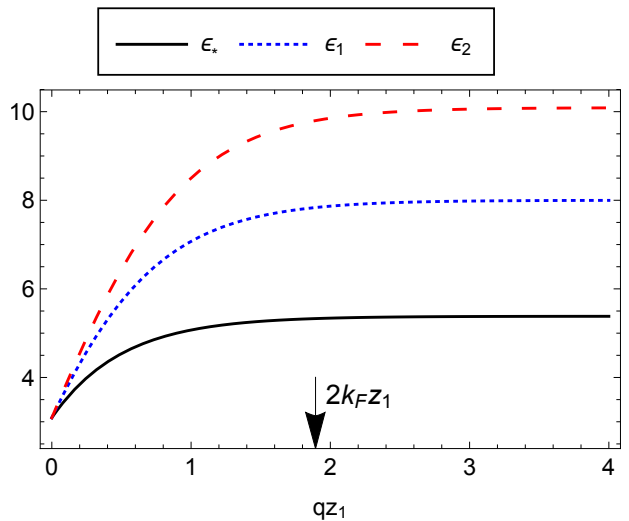


FIG. 1. High frequency (static) dielectric constants, ϵ_* , ϵ_1 and ϵ_2 with respect to wavevector. We take $\epsilon_{\text{STO}} = 5.18$, and $\epsilon_{\text{FeSe}} = 15$.

The ionic contribution to the dielectric function is well approximated by

$$\epsilon_{ion}(q, \Omega) = \epsilon_1 \left[1 - e^{-2qz_1} \sum_a \frac{\gamma_a \Omega_a^2}{\Omega^2 + \Omega_a^2} \right]^{-1} \quad (7)$$

where the Ω_a are the frequencies of the longitudinal optic modes of SrTiO₃ as appropriately modified by the presence of the surface. The shifts of phonon frequencies due to the surface, the effect of the internal electric fields arising from the doped FeSe and the corresponding depletion region of the STO, and the other dielectric effects associated with spatial symmetry breaking are parametrized by ϵ_2 and ϵ_* are included into the mode-dependent parameter γ_a . The parameters $\gamma_a = 0.002, 0.104, 0.854$ for $a = 1, 2, 3$ are chosen to be consistent with bulk STO and to produce a dielectric constant that coincides with our previous work¹⁷, in which $\epsilon(0, 0) \approx 100$ was obtained for the near-interface region. The key feature of this result is the exponential dependence of the screening on momentum, shown in Fig. 2 for parameters representative of FeSe on STO.

III. ELECTRONIC DENSITY FLUCTUATIONS: RPA SCREENING AND FINAL EFFECTIVE INTERACTION

The interaction in Eq. 6 is screened by electronic density fluctuations, which we treat here at the random phase approximation (RPA) level, leading to the final interaction

$$V^*(q, \Omega) = \frac{V_{\text{eff}}(q, \Omega)}{1 - \chi_0(q, \Omega) V_{\text{eff}}(q, \Omega)} \quad (8)$$

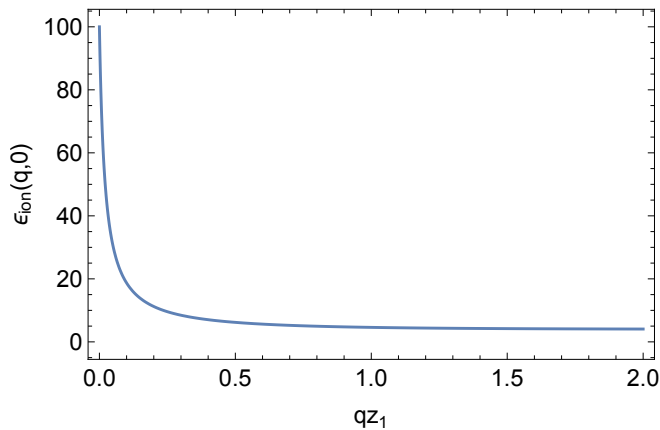


FIG. 2. $\epsilon_{ion}(q, \Omega)$ for zero frequency calculated for $2k_F z_1 = 1.89$ representative of FeSe on STO.

with χ_0 the free electron approximation to the electronic polarizability. We calculate χ_0 in two dimensions and Matsubara frequency assuming two parabolic bands representing the two zone-face-centered electron bands of FeSe:

$$\chi_0(q, \Omega) = 4 \int \frac{kd\theta}{4\pi^2} \frac{f(\epsilon_{k-\frac{q}{2}}) - f(\epsilon_{k+\frac{q}{2}})}{i\Omega + \epsilon_{k-\frac{q}{2}} - \epsilon_{k+\frac{q}{2}}} \equiv -N_0\Phi(q, \Omega) \quad (9)$$

with the prefactor 4 expressing the spin and valley degeneracy of the electrons and total density of states $N_0 = 2m/\pi$ with m the electron mass.

It is convenient to work in dimensionless units, defining

$$\bar{q} = \frac{q}{2k_F} \quad (10)$$

$$\bar{z} = 4k_F z_1 \quad (11)$$

$$\bar{\Omega} = \frac{\Omega}{4E_F} \quad (12)$$

with $E_F = k_F^2/(2m)$. We also introduce the gas parameter $r_S = 2/a_B^* k_F$ where $a_B^* = \epsilon_1/me^2$ is the effective Bohr radius. In our previous work¹⁷, we found for band parameters appropriate to monolayer FeSe on SrTiO₃ $m \approx m_e$, and $k_F \approx 0.22/\text{\AA}$ so $E_F \approx 0.1\text{eV}$ (strong correlation effects may reduce this value). With $\epsilon_1 \approx 3$ for small wavevectors, we have $a_B^* \approx 3a_B$, and so $r_S \approx 6$. We also rescale all dielectric functions by ϵ_1 and denote the rescaled functions with tildes (e.g. $\tilde{\epsilon}_{ion} = \frac{\epsilon_{ion}}{\epsilon_1}$), so

We then define a dimensionless interaction $v^* = N_0 V^*$ and obtain

$$v^*(q, \Omega) = \frac{\frac{r_S}{\bar{q}\tilde{\epsilon}_{ion}}}{1 + \frac{r_S}{\bar{q}\tilde{\epsilon}_{ion}}\Phi} = \frac{r_S}{\bar{q}\tilde{\epsilon}_{tot}} \quad (13)$$

with

$$\tilde{\epsilon}_{tot} = \tilde{\epsilon}_{RPA} + \tilde{\epsilon}_{ion} - 1 \quad (14)$$

$$\tilde{\epsilon}_{RPA} = 1 + \frac{r_S}{\bar{q}}\Phi \quad (15)$$

IV. PLASMON

Plasmon frequencies are zeros of the total dielectric function, in other words frequencies $\omega_{pl}(q)$ satisfying

$$\epsilon_{tot}(q, \omega_{pl}(q)) = 0 \quad (16)$$

Using Eqs. 7 and 15 and adopting the small- q limit form for Φ we obtain for the plasmon dispersion

$$\frac{r_S}{\bar{q}} \left(1 - \frac{\bar{\omega}_{pl}}{\sqrt{\bar{\omega}_{pl}^2 - \bar{q}^2}} \right) + \left[1 - \gamma e^{-\bar{q}\bar{z}} \sum_a \frac{\bar{\Omega}_a^2}{\bar{\Omega}_a^2 - \bar{\omega}_{pl}^2} \right]^{-1} = 0 \quad (17)$$

Note that for $\bar{q} > \bar{\omega}_{pl}$ the plasmon enters the particle-hole continuum and becomes overdamped and Eq. 17, which gives the dispersion for undamped plasmons, does not apply.

Let us first consider the limit $\bar{\omega}_{pl} \ll \bar{\Omega}_a$, in which case $\bar{q} \ll \bar{\omega}_{pl}$, the last term is approximately $(\tilde{\epsilon}_{ion}(0, 0)^{-1} + \bar{q}\bar{z})^{-1}$ with $\tilde{\epsilon}_{ion}(0, 0) \gg 1$ and we have, approximately

$$\bar{\omega}_{pl}^2 = \frac{r_S \bar{q}}{2\tilde{\epsilon}_{ion}(0, 0)} + \frac{r_S \bar{z}}{2} \bar{q}^2 \quad (18)$$

Thus at very low energies and long wavelengths we have a conventional 2D plasmon with square root dispersion determined by the long wavelength dielectric constant, which is large. At the scale $\bar{q}_z \approx 1/(\tilde{\epsilon}_{ion}(0, 0)\bar{z})$ the wavevector dependence of the dielectric function (arising from the set-back of the FeSe layer from the SrTiO₃) becomes important and the dispersion becomes linear in wavevector. However, when ω_{pl} becomes comparable to the lowest optic phonon frequency, the frequency dependence of the dielectric function becomes important and the dispersion changes.

Band theory for the monolayer FeSe on STO¹⁷ gives $r_S = 5.7$, $\bar{z} = 3.8$, $\tilde{\epsilon}(0, 0)^{-1} = 0.04$. The lowest important phonon frequency $\bar{\Omega}_1 \approx 0.025$ so the momentum at which the plasmon crosses the phonon is about $\bar{q} \sim 0.005$; at this scale the quadratic term in Eq. 18 is small so the regime of linearly dispersing plasmons is obscured by the phonon bands.

At frequencies above the highest phonon frequency the plasmon dispersion crosses over to the standard unrenormalized square-root dispersion. Compared to the long wavelength case, the only difference is the dielectric constant, which enters the frequency as the square root, so the dispersion curve is changed by a factor of about 4. Fig. 3 shows the locus of the zeros of the dielectric function for the band parameters obtained in our previous work¹⁷. The renormalized plasmon is visible only at the very lowest frequencies.

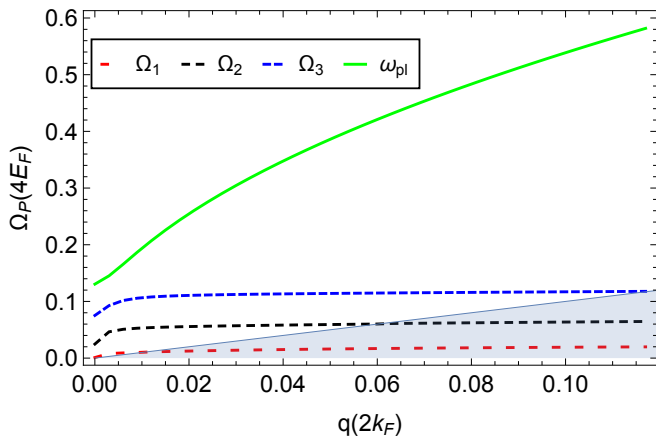


FIG. 3. Collective mode dispersions with the interaction with the STO LO modes for $r_S = 5.7$, $\bar{z} = 4k_F z_1 = 3.89$. The shaded region represents the particle-hole continuum.

V. INTERACTION

There are various ways to view the combined electron-electron and electron-ion interactions. For a first approach we follow the theory of electron-phonon interactions in semiconductors^{18,19} and define the electron-phonon interaction as the difference between the total interaction and the purely electronic (here RPA) parts

$$v^*(q, \Omega) = v_{\text{RPA}}(q, \Omega) - v_{ph}(q, \Omega) \quad (19)$$

where

$$v_{\text{RPA}} = \frac{\frac{r_S}{\bar{q}}}{1 + \frac{r_S}{\bar{q}}\Phi} = \frac{1}{\frac{\bar{q}}{r_S} + \Phi} \equiv \frac{r_S}{\bar{q}\tilde{\epsilon}_{\text{RPA}}} \quad (20)$$

and (note the standard sign convention for which a positive v_{ph} is an attractive interaction)

$$v_{ph} = v_{\text{RPA}} \frac{\tilde{\epsilon}_{\text{tot}} - \tilde{\epsilon}_{\text{RPA}}}{\tilde{\epsilon}_{\text{tot}}} = v_{\text{RPA}} \frac{\frac{\bar{q}}{r_S} (1 - \tilde{\epsilon}_{\text{ion}}^{-1})}{\frac{\bar{q}}{r_S} + \tilde{\epsilon}_{\text{ion}}^{-1}\Phi} \quad (21)$$

Refs. 18 and 19 argued that the v_{RPA} term should be viewed as the RPA-screened electron-phonon coupling. However, in the present case the imaginary part of v_{ph} changes sign as the frequency is varied, it cannot be interpreted as the longitudinal phonon propagator renormalized by coupling to electrons (see Appendix C for details).

In a conventional metal, $\tilde{\epsilon}$ has negligible momentum dependence, and is different from unity only for frequencies less than the longitudinal optic phonon frequency. For these frequencies, for all momenta except for the very narrow range $q < \Omega_{LO}/v_F$ we may set $\Phi = 1$. For typical $\tilde{\epsilon}$ values somewhat larger than 1 and typical metallic $r_S \sim 2$ we find a dimensionless interaction of the order of (but somewhat smaller than) unity. Thus in many conventional superconductors longitudinal modes make

some contribution to pairing but the transverse modes, which are not screened, make a larger contribution.

To understand the differences arising in the present situation it is useful to consider a simplified situation in which there is only one optic phonon mode (bare frequency Ω_{LO}) and assume that the host material is tuned exactly to the ferroelectric instability $\gamma = 1$. Then we may rewrite Eq. 21 using Eq. 7 as (in the denominator we approximated $1 - e^{-\bar{q}z} \rightarrow \bar{q}z$)

$$v_{ph} = v_{\text{RPA}} \frac{e^{-\bar{q}z}\bar{\Omega}_{LO}^2}{\bar{\Omega}^2 \left(1 + \frac{r_S}{\bar{q}}\Phi\right) + \bar{\Omega}_{LO}^2 (1 + r_S\bar{z}\Phi)} \quad (22)$$

As expected, the interaction is confined to momenta less than or of order of $\bar{z}^{-1} \approx 0.25$. The frequencies $\bar{\Omega} = \bar{q}$ corresponding to these momenta are of the order of the highest phonon frequency. Thus on the Matsubara axis, for $\bar{\Omega} \lesssim \bar{q}$, Φ and $v_{\text{RPA}} \approx 1$ and the phonon contribution of the interaction v_{ph} is approximately $1/r_S\bar{z} \lesssim 0.04$ using the band parameters mentioned above. These qualitative conclusions are confirmed by the two panels of Fig. 4 which show the r_S and momentum dependence of v_{ph} at zero Matsubara frequency. We see that the interaction is enhanced at small momentum and small r_S but is never even as large as unity.

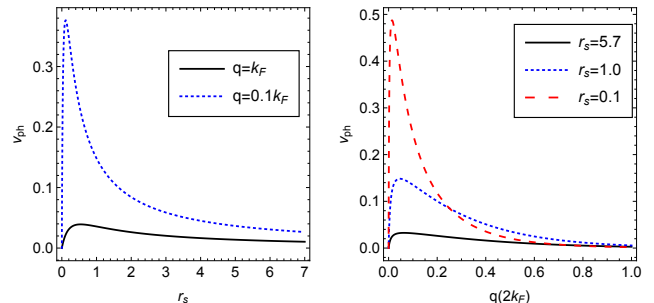


FIG. 4. Zero frequency v_{ph} , left: as a function of r_S , and right: as a function of q .

For larger $\bar{\Omega}$ and smaller \bar{q} , Φ becomes small, v_{RPA} becomes larger while the percentage of the v_{ph} in the total interaction is reduced. To obtain a significant interaction one must achieve a much smaller set-back distance, so that $\tilde{\epsilon}$ is large even for $\bar{q} \sim 1$ and have more weakly correlated electron gas (smaller r_S). This qualitative analysis is confirmed by the detailed numerics presented in Fig. 5. Thus in effect electronic screening strongly reduces the interaction, so very little significant effect of phonons on electronic properties remains.

VI. REPLICA BANDS

Recent photoemission experiments have reported replica bands in monolayer FeSe on STO⁹. A replica

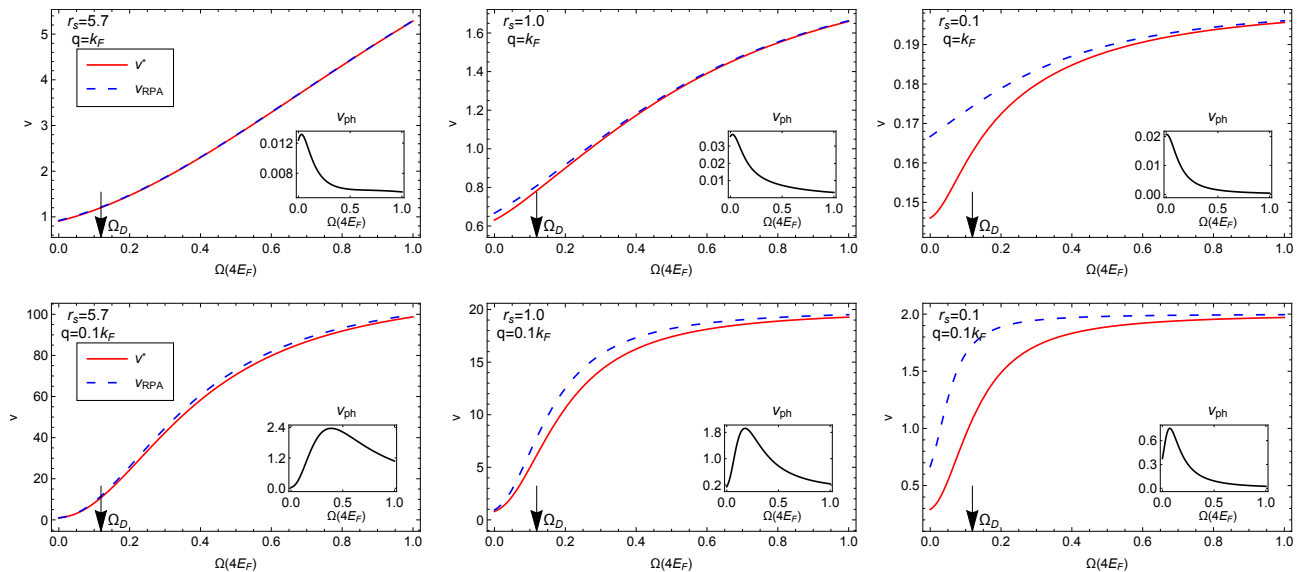


FIG. 5. Dimensionless interaction plotted as function of frequency for q and r_s -values shown. The insets show the relevant phonon-induced attractive interactions v_{ph} . Ω_D , the highest and dominant LO phonon frequency, label the arrows on the frequency axes.

band is an image of the main band, shifted to a higher binding energy by a momentum independent energy. Replica bands are obtained theoretically in electron-boson calculations involving an extreme forward-scattering limit¹¹ and it was suggested that coupling to STO dipolar phonons could satisfy the necessary conditions.

Here for simplicity we discuss the replica bands by calculating the electron self energy to leading order in the interaction:

$$\Sigma(k, \omega) = \int dv \frac{d^2q}{(2\pi)^3} G^0(k+q, \omega+\nu) V^*(q, \nu) \quad (23)$$

with G^0 the free electron Green's function. In the extreme forward scattering limit and on the Matsubara axis

$$V_{\text{forward}}^* = g_0^2 \delta^2(q) \frac{2\Omega_0}{\nu^2 + \Omega_0^2} \quad (24)$$

so analytically continuing

$$\Sigma_{\text{forward}}(k, \omega) = \frac{g_0^2 n_f}{\omega - (\varepsilon_k - \Omega_0) - i\delta} + \frac{g_0^2 (1 - n_f)}{\omega - (\varepsilon_k + \Omega_0) - i\delta} \quad (25)$$

with n_f the Fermi function.

In the upper and lower left panels of Fig. 6 we show the spectral function computed using Eq. 25 for a line through the M point (center of the electron pocket). The main peak is the quasiparticle energy, and the replica band is visible at higher binding energy. The distance between the main peak and the shakeoff peak is dependent on the electron-phonon interaction matrix¹¹.

Fig. 7 shows the low frequency behavior of the real and imaginary parts of total interaction computed for

FeSe/STO, computed using a simplified model in which only the highest frequency phonon is retained. We see that the interaction has considerable structure as a function of momentum and energy, and is not particularly peaked at small momentum. For this reason, the interactions (which are essentially the same as in the absence of phonons), produce a wide tail in the energy dispersion curve but no replica bands.

Indeed, replica bands are not always reported in experiments monolayer FeSe on STO with superconducting T_c greater than 60K, the replica bands are not always reported. Thus it is possible that certain surface treatments change the surface electronic states. Our calculation shows that replica bands are not a natural consequence of a coupling between substrate dipolar phonons and electrons in the monolayer.

VII. SUMMARY

We have studied the coupling of dipole active (LO) phonons in the depletion regime of SrTiO₃ to electrons in a monolayer of FeSe. LO phonons produce a dipole field which is long ranged, allowing many STO phonon modes to couple to the electrons in the FeSe. However, because the coupling is Coulombic, it is screened by the total charge density fluctuations in FeSe. At the RPA level, we find that the electron fluctuations in FeSe screen most of the electron-phonon interaction, leaving the overall phonon-mediated potential very weak, and unable either to produce a significant contribution to superconductivity or to cause the “shadow bands” observed in recent experiments. We therefore conclude that some other

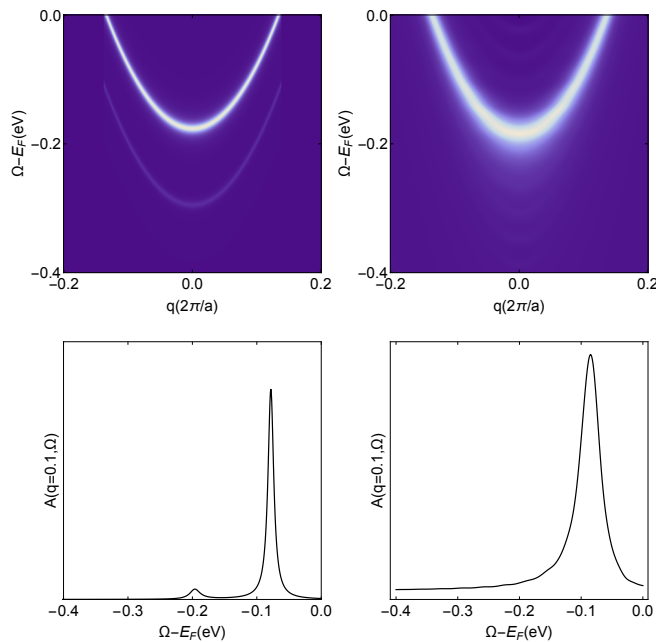


FIG. 6. Electron spectral function computed for idealized delta-function forward scattering model (Eq. 25 (left panels) and physical electron-phonon coupling (right panels). Top panels: greyscale (color online) representation of spectral function as function of frequency and of wavevector along $\Gamma - M - \Gamma$. Bottom panels: energy dispersion curves computed at $q = 0.1(2\pi/a)$ away from M point. The self energy is calculated from Eq. 23 with the frequency integration cut at $|\omega'| = 20$ eV and 64×64 q points within the Fermi surface. Here a is the lattice constant of the physical (2Fe) Brillouin zone.

(perhaps non-phonon) mechanism is responsible for the observed enhancement of the transition temperature.

Our calculations were performed within the RPA approximation, which captures the long range Coulomb effects but is not quantitatively accurate in the strongly correlated, low electron density situation relevant to FeSe. It is possible that a more sophisticated calculation including vertex corrections²⁰ and a better treatment of the electronic screening in the low density limit might change the physics. Finally, our analyses do not rule out other possibilities that do not couple to the total electron density fluctuations, for example magnetic or nematic fluctuations²¹.

VIII. ACKNOWLEDGEMENT

YZ is grateful to L-F. Arsenault, Z. He, D. Kennes, J. Liu and E. Wilner for helpful discussions. Computations were carried out on the Yeti High Performance Computing (HPC) Cluster at Columbia University. YZ is supported by the Cornell Center for Materials Research with funding from the NSF MRSEC program (DMR-1120296) AJM is supported by DOE-ER-046169. We appreciate

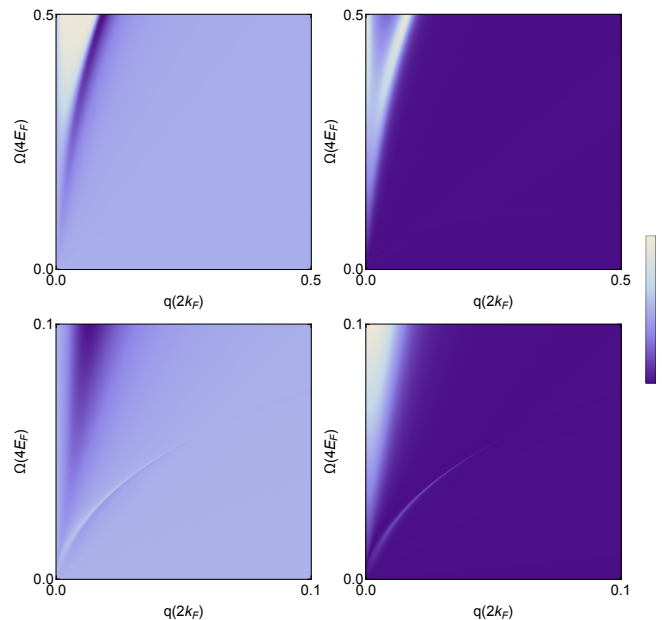


FIG. 7. Greyscale plot of magnitude of dimensionless inter-action v^* computed in plane of momentum and real frequency using the simplified model containing only the the highest LO phonon at $r_S = 5.7$. Left, real part. Right: imaginary part. Bottom panels are the zoomed in parts of the upper panels for small wavevectors.

an anonymous referee for pointing out the error in the original Eq. 25.

Appendix A: Electrostatic problem and boundary conditions

We set up the interface normal to z direction. STO substrate fills the $z < 0$ semi-space with high frequency dielectric constant ϵ_{STO} , and the dipoles \vec{d} live in the STO depletion layer that starts at $z = 0$ and extends to negative z_0 , the width of depletion region¹⁷. In general each unit cell contains N frozen dipoles (for STO $N = 3$). Each dipole has an effective dipole moment Z_i with $i = 1 \dots N$. FeSe monolayer is modeled within the $0 < z < z_1$ layer, with high frequency dielectric constant ϵ_{FeSe} and a two-dimensional charge density at $z = z_1$, $\rho(\vec{r}) = \rho_{2D}(r_{2D})\delta(z - z_1)$. $z > z_1$ space is vacuum. Here for simplicity we assume the high frequency dielectric constant for the space between STO and the FeSe sheet is the same with ϵ_{FeSe} . In-plane Fourier transform a three dimensional Coulomb potential leaves the out-of-plane dimension in a exponential factor $\exp(-qz)$.

The static Hamiltonian is

$$H_{\text{Coul}} = \int \frac{d^3r}{a^3} \rho(r)\Phi^e(r) + \rho(r)\Phi^d(r) + \sum_i Z_i \vec{d}_i(r) \cdot \nabla \Phi^e(r) + \sum_i Z_i \vec{d}_i(r) \cdot \nabla \Phi^d(r) \quad (\text{A1})$$

Here we define the charge density and dipole density with respect to the lattice constant of STO a , and thus there are two Fe per unitcell. Φ^e and Φ^d denote the effective potential generated by electrons and dipoles, respectively.

So for the effective potential of electrons, we can assume

$$\Phi^e = \begin{cases} \Phi_3^e e^{-q(z-z_1)}, & z > z_1 \\ \Phi_2^{e+} e^{q(z-z_1)} + \Phi_2^{e-} e^{-q(z-z_1)}, & 0 < z < z_1 \\ \Phi_1^e e^{q(z-z_1)}, & z < 0 \end{cases} \quad (\text{A2})$$

with Φ_i to be determined by boundary conditions.

At $z = z_1$, we have

$$\Phi_3^e = \Phi_2^{e+} + \Phi_2^{e-} \quad (\text{A3})$$

$$q\Phi_3^e + \epsilon_{\text{FeSe}} q(\Phi_2^{e+} - \Phi_2^{e-}) = 4\pi\rho_q \quad (\text{A4})$$

At $z = 0$,

$$\Phi_1^e e^{-qz_1} = \Phi_2^{e+} e^{-qz_1} + \Phi_2^{e-} e^{qz_1} \quad (\text{A5})$$

$$-q\Phi_1^e \epsilon_{\text{STO}} e^{-qz_1} = -q\epsilon_{\text{FeSe}}(\Phi_2^{e+} e^{-qz_1} - \Phi_2^{e-} e^{qz_1}) \quad (\text{A6})$$

Solving equations above gives

$$\Phi^e = \begin{cases} \left(1 - e^{-2qz_1} \frac{\epsilon_{\text{STO}} - \epsilon_{\text{FeSe}}}{\epsilon_{\text{STO}} + \epsilon_{\text{FeSe}}}\right) e^{-q(z-z_1)} \Phi_{2+}^e, & z > z_1 \\ \left[e^{q(z-z_1)} - e^{-q(z+z_1)} \frac{\epsilon_{\text{STO}} - \epsilon_{\text{FeSe}}}{\epsilon_{\text{STO}} + \epsilon_{\text{FeSe}}} \right] \Phi_{2+}^e, & 0 < z < z_1 \\ \frac{2\epsilon_{\text{FeSe}}}{\epsilon_{\text{STO}} + \epsilon_{\text{FeSe}}} e^{q(z-z_1)} \Phi_{2+}^e, & z < 0 \end{cases} \quad (\text{A7})$$

with

$$\Phi_{2+}^e = \frac{4\pi\rho_q}{q} \left[(\epsilon_{\text{FeSe}} + 1) + (\epsilon_{\text{FeSe}} - 1) \frac{\epsilon_{\text{STO}} - \epsilon_{\text{FeSe}}}{\epsilon_{\text{STO}} + \epsilon_{\text{FeSe}}} e^{-2qz_1} \right]^{-1} \quad (\text{A8})$$

Similarly, in-plane Fourier transform the dipole field generated by the semi-infinite space of STO also gives exp $(-qz)$ factor for the out-of-plane dimension. We write

$$\Phi^d = \begin{cases} \Phi_3^d e^{-qz}, & z > z_1 \\ \Phi_2^{d+} e^{qz} + \Phi_2^{d-} e^{-qz}, & 0 < z < z_1 \\ \Phi_1^d e^{qz}, & z < 0 \end{cases} \quad (\text{A9})$$

with boundary conditions at $z = z_1$,

$$\Phi_3^d e^{-qz_1} = \Phi_2^{d+} e^{qz_1} + \Phi_2^{d-} e^{-qz_1} \quad (\text{A10})$$

$$-q\Phi_3^d e^{-qz_1} = \epsilon_{\text{FeSe}} q(\Phi_2^{d+} e^{qz_1} - \Phi_2^{d-} e^{-qz_1}) \quad (\text{A11})$$

and at $z = 0$,

$$\Phi_2^{d+} + \Phi_2^{d-} = \Phi_1^d \quad (\text{A12})$$

$$-q\epsilon_{\text{FeSe}}(\Phi_2^{d+} - \Phi_2^{d-}) + q\epsilon_{\text{STO}}\Phi_1^d = \sum_i Z_i d_q^i \quad (\text{A13})$$

These lead to

$$\Phi^d = \begin{cases} \frac{2\epsilon_{\text{FeSe}}}{\epsilon_{\text{FeSe}} + 1} \Phi_{2-}^d e^{-qz}, & z > z_1 \\ \left(e^{-qz} + \frac{\epsilon_{\text{FeSe}} - 1}{\epsilon_{\text{FeSe}} + 1} e^{q(z-2z_1)} \right) \Phi_{2-}^d, & 0 < z < z_1 \\ \left(1 + \frac{\epsilon_{\text{FeSe}} - 1}{\epsilon_{\text{FeSe}} + 1} e^{-2qz_1} \right) \Phi_{2-}^d e^{qz}, & z < 0 \end{cases} \quad (\text{A14})$$

with

$$\Phi_{2-}^d = \frac{4\pi \sum_i Z_i e d_i(q, 0)}{q} \times \left[(\epsilon_{\text{STO}} + \epsilon_{\text{FeSe}}) + (\epsilon_{\text{STO}} - \epsilon_{\text{FeSe}}) \frac{\epsilon_{\text{FeSe}} - 1}{\epsilon_{\text{FeSe}} + 1} e^{-2qz_1} \right]^{-1} \quad (\text{A15})$$

From the above electric potentials, we can write the interaction terms as

$$H_{e-d} = \int \frac{d^2q}{(2\pi)^2} \frac{2\pi e^2 \sum_i Z_i \rho_q d_{-q}^i e^{-qz_1}}{q\epsilon_\star} \quad (\text{A16})$$

$$H_{d-e} = \int \frac{d^2q}{(2\pi)^2} \frac{2\pi e^2 \sum_i Z_i \rho_{-q} d_q^i e^{-qz_1}}{q\epsilon_\star} \quad (\text{A17})$$

where the interactions have been summed over z , with q here in-plane. ϵ_\star expresses the effective dielectric constant associated to the interacting electron-dipole fields,

$$\epsilon_\star = \frac{1}{4\epsilon_{\text{FeSe}}} \left[(\epsilon_{\text{STO}} + \epsilon_{\text{FeSe}})(\epsilon_{\text{FeSe}} + 1) + (\epsilon_{\text{STO}} - \epsilon_{\text{FeSe}})(\epsilon_{\text{FeSe}} - 1) e^{-2qz_1} \right] \quad (\text{A18})$$

This value varies between $(\epsilon_{\text{STO}} + 1)/2$, for $qz_1 = 0$ where the case reduces to the surface of a dielectrics, and $(\epsilon_{\text{STO}} + \epsilon_{\text{FeSe}})(\epsilon_{\text{FeSe}} + 1)/4\epsilon_{\text{FeSe}}$ for $qz_1 \rightarrow \infty$.

Thus in reciprocal space we may write the static Hamiltonian,

$$H_{\text{Coul}} = \frac{1}{2} \int \frac{d^3q}{(2\pi)^3} \frac{4\pi e^2}{\epsilon_1 q^2} \rho_q \rho_{-q} + iq \frac{4\pi e^2 e^{-q_{\parallel} z_1}}{q^2 \epsilon_\star} \sum_m (Z_m d_{-q}^m \rho_q - Z_m d_q^m \rho_{-q}) + \sum \frac{4\pi Z_i Z_j e^2}{a\epsilon_2} d_q^i d_{-q}^j \quad (\text{A19})$$

where q is a 3D momentum and q_{\parallel} is the in-plane component. ϵ_1 and ϵ_2 represent the effective dielectric functions

$$\epsilon_1 = \epsilon_\star \left(\frac{2\epsilon_{\text{FeSe}}}{\epsilon_{\text{STO}} + \epsilon_{\text{FeSe}}} \right) \left(1 - e^{-2qz_1} \frac{\epsilon_{\text{STO}} - \epsilon_{\text{FeSe}}}{\epsilon_{\text{STO}} + \epsilon_{\text{FeSe}}} \right)^{-1} \quad (\text{A20})$$

$$\epsilon_2 = \epsilon_\star \left(\frac{2\epsilon_{\text{FeSe}}}{1 + \epsilon_{\text{FeSe}}} \right) \left(1 + e^{-2qz_1} \frac{\epsilon_{\text{FeSe}} - 1}{\epsilon_{\text{FeSe}} + 1} \right)^{-1} \quad (\text{A21})$$

For $qz_1 = 0$ ϵ_1 and ϵ_2 reduce to $(\epsilon_{\text{STO}} + 1)/2$, resemble to the dielectric constant at the interface of vacuum and a semi-infinite STO. For $qz_1 \rightarrow \infty$, they reduce to $(\epsilon_{\text{STO}} + 1)/2$ and $(\epsilon_{\text{FeSe}} + \epsilon_{\text{STO}})/2$, respectively.

Appendix B: Decoupling the phonons

Next we include the energy of multiple dipole oscillations that contribute to the dynamic energy

$$H_d = \frac{1}{2} \int \frac{d^3r}{a^3} \sum_{ij} K_{ij} d_i(r) d_j(r) + M_{ij} \dot{d}_i(r) \dot{d}_j(r) \quad (\text{B1})$$

with K and M the force and mass matrices for transverse optical phonons that are nonpolar. The lowest eigenvalue of K goes to zero at the ferroelectric transition.

Combining H_{Coul} and H_d , we have

$$H = \frac{1}{2} \int \frac{d^3q}{(2\pi)^3} \frac{4\pi e^2}{\epsilon_1 q^2} \rho_q \rho_{-q} + iq \frac{4\pi e^2 e^{-q_{\parallel} z_1}}{q^2 \epsilon_{\star}} \sum_i (Z_i d_{-q}^i \rho_q - Z_i d_q^i \rho_{-q}) + \sum_{ij} \left(K_{ij} + \frac{4\pi Z_i Z_j e^2}{a \epsilon_2} - M_{ij} \Omega^2 \right) d_q^i d_{-q}^j \quad (\text{B2})$$

To decouple the dynamic phonon term, we shift the dipoles as

$$d_q^i \rightarrow d_q^i + i \rho_q \frac{4\pi Z_i e^2 e^{-q_{\parallel} z_1}}{q \epsilon_{\star}} \mathcal{D} \quad (\text{B3})$$

where we define

$$\mathcal{D} = \left(K_{ij} + \frac{4\pi Z_i Z_j e^2}{a \epsilon_2} - M_{ij} \Omega^2 \right)^{-1} \quad (\text{B4})$$

\mathcal{D} can be viewed as the longitudinal phonon propagator in STO, with the dipole-dipole Coulomb energy term leading to the large LO-TO splitting in STO²².

Summing over q_z using the $q_z = iq$ pole, the electron density part Hamiltonian becomes

$$H_{el} = \frac{1}{2} \int \frac{d^2q}{(2\pi)^2} \frac{2\pi e^2}{q \epsilon_1} \rho_q \rho_{-q} \left(1 - \frac{4\pi e^2 e^{-2q z_1}}{\epsilon_2} \sum_{ij} Z_i \mathcal{D}_{ij} Z_j \right) = \frac{1}{2} \int \frac{d^2q}{(2\pi)^2} \rho_q \rho_{-q} V_{\text{eff}}(q, \Omega) \quad (\text{B5})$$

where the \parallel subscript is dropped since we are now in the 2D momentum space.

Appendix C: Comparing to conventional theory

Comparing to Eq. (9) in Ref 19, we rewrite Eq 8 as

$$V^{\star} = V_c \frac{1 - e^{-2q z_1} g^2 D / V_c}{1 - \chi_0 (V_c - e^{-2q z_1} g^2 D)}$$

$$= \frac{V_c}{\epsilon_{\text{RPA}}} - V_c \left[\epsilon_{\text{RPA}}^{-1} - \frac{1}{\epsilon_{\text{RPA}} + \frac{1}{\frac{e^{-2q z_1} D}{1 - e^{-2q z_1} D}}} \right] = \frac{V_c}{\epsilon_{\text{RPA}}} \left[1 - \frac{D^{\star}}{\epsilon_{\text{RPA}} + D^{\star}} \right] \quad (\text{C1})$$

with the renormalized phonon ‘‘propagator’’ and electron-phonon interaction strength g ,

$$g^2 D = \frac{2\pi e^2}{\epsilon_1 q} \sum_a \frac{\gamma_a \Omega_a^2}{\Omega_a^2 + \Omega^2} \quad (\text{C2})$$

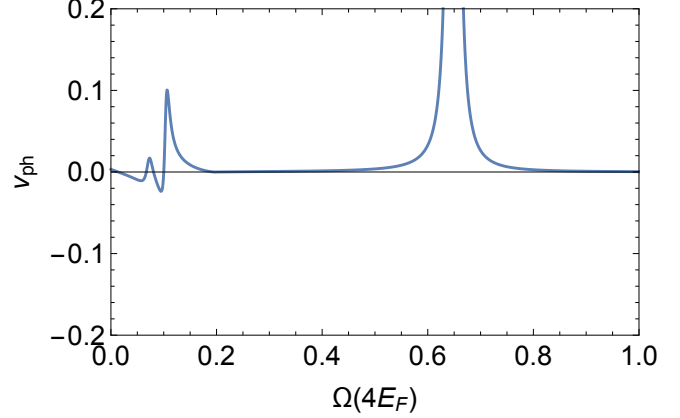


FIG. A1. Imaginary part of v_{ph} in real frequency. $\bar{q} = 0.2$, $r_S = 5.7$, $z_1 = 1.89$. The strong peak near $\bar{\Omega} = 0.6$ denotes the plasmon. The peaks near $\bar{\Omega} = 0.1$ show the poles of phonons.

and

$$D^{\star} = \frac{e^{-2q z_1} D}{1 - e^{-2q z_1} D} \quad (\text{C3})$$

the dressed phonon ‘‘propagator’’ that decay with the set back distance z_1 , and

$$\epsilon_{\text{RPA}} = 1 - \chi_0 V_c \quad (\text{C4})$$

the electronic part of the dielectric constant.

The first term in Eq. C1 gives the RPA-screened Coulomb interaction, $V_{\text{RPA}} = V_c / \epsilon_{\text{RPA}}$, while the second term contains the screened phonon-induced attractive interaction that may lead to superconductivity.

The v_{ph} in the main text is exactly the dimensionless form of the second term. However, we have to note that v_{ph} should not be thought as conventional propagators. Fig. A1 shows the imaginary part of v_{ph} in real frequency. Besides the plasmon peak, the imaginary part changes sign near the poles of LO phonons. The existence of this effect is independent of wavevector.

¹ W. Qing-Yan, L. Zhi, Z. Wen-Hao, Z. Zuo-Cheng, Z. Jin-Song, L. Wei, D. Hao, O. Yun-Bo, D. Peng, C. Kai,

W. Jing, S. Can-Li, H. Ke, J. Jin-Feng, J. Shuai-Hua, W. Ya-Yu, W. Li-Li, C. Xi, M. Xu-Cun, and X. Qi-Kun,

- Chin. Phys. Lett.* **29**, 037402 (2012).
- ² S. He, J. He, W. Zhang, L. Zhao, D. Liu, X. Liu, D. Mou, Y.-B. Ou, Q.-Y. Wang, Z. Li, L. Wang, Y. Peng, Y. Liu, C. Chen, L. Yu, G. Liu, X. Dong, J. Zhang, C. Chen, Z. Xu, X. Chen, X. Ma, Q. Xue, and X. J. Zhou, *Nat. Mater.* **12**, 605 (2013).
 - ³ J.-F. Ge, Z.-L. Liu, C. Liu, C.-L. Gao, D. Qian, Q.-K. Xue, Y. Liu, and J.-F. Jia, *Nat. Mater.* **14**, 285 (2015).
 - ⁴ S. Tan, Y. Zhang, M. Xia, Z. Ye, F. Chen, X. Xie, R. Peng, D. Xu, Q. Fan, H. Xu, J. Jiang, T. Zhang, X. Lai, T. Xiang, J. Hu, B. Xie, and D. Feng, *Nat. Mater.* **12**, 634 (2013).
 - ⁵ Y. Miyata, K. Nakayama, K. Sugawara, T. Sato, and T. Takahashi, *Nat. Mater.* **14**, 775 (2015).
 - ⁶ W. H. Zhang, X. Liu, C. H. P. Wen, R. Peng, S. Y. Tan, B. P. Xie, T. Zhang, and D. L. Feng, *Nano Lett.* **16**, 1969 (2016), PMID: 26859620.
 - ⁷ B. Lei, J. H. Cui, Z. J. Xiang, C. Shang, N. Z. Wang, G. J. Ye, X. G. Luo, T. Wu, Z. Sun, and X. H. Chen, *Phys. Rev. Lett.* **116**, 077002 (2016).
 - ⁸ H. Ding, Y.-F. Lv, K. Zhao, W.-L. Wang, L. Wang, C.-L. Song, X. Chen, X.-C. Ma, and Q.-K. Xue, *Phys. Rev. Lett.* **117**, 067001 (2016).
 - ⁹ J. J. Lee, F. T. Schmitt, R. G. Moore, S. Johnston, Y. T. Cui, W. Li, M. Yi, Z. K. Liu, M. Hashimoto, Y. Zhang, D. H. Lu, T. P. Devereaux, D. H. Lee, and Z. X. Shen, *Nature* **515**, 245 (2014).
 - ¹⁰ D.-H. Lee, *Chinese Physics B* **24**, 117405 (2015).
 - ¹¹ L. Rademaker, Y. Wang, T. Berlijn, and S. Johnston, *New J. Phys.* **18**, 022001 (2016).
 - ¹² L. P. Gor'kov, *Phys. Rev. B* **93**, 060507 (2016).
 - ¹³ J. C. Inkson and P. W. Anderson, *Phys. Rev. B* **8**, 4429 (1973).
 - ¹⁴ R. H. Yuan, W. D. Kong, L. Yan, H. Ding, and N. L. Wang, *Phys. Rev. B* **87**, 144517 (2013).
 - ¹⁵ R. Viana, P. Lunkenheimer, J. Hemberger, R. Böhmer, and A. Loidl, *Phys. Rev. B* **50**, 601 (1994).
 - ¹⁶ R. C. Neville, B. Hoeneisen, and C. A. Mead, *J. Appl. Phys.* **43**, 2124 (1972).
 - ¹⁷ Y. Zhou and A. J. Millis, *Phys. Rev. B* **93**, 224506 (2016).
 - ¹⁸ B. B. Varga, *Phys. Rev.* **137**, A1896 (1965).
 - ¹⁹ C. S. Koonce, M. L. Cohen, J. F. Schooley, W. R. Hosler, and E. R. Pfeiffer, *Phys. Rev.* **163**, 380 (1967).
 - ²⁰ Y. Yamakawa and H. Kontani, arXiv: **1611.05375** (2016).
 - ²¹ J. Kang and R. M. Fernandes, *Phys. Rev. Lett.* **117**, 217003 (2016).
 - ²² W. Zhong, R. D. King-Smith, and D. Vanderbilt, *Phys. Rev. Lett.* **72**, 3618 (1994).